Chemical Engineering Journal 162 (2010) 792–801

Contents lists available at ScienceDirect

Chemical Engineering Journal

journal homepage: www.elsevier.com/locate/cej

Prediction of drop sizes for liquid–liquid systems in stirred slim reactors—Part I: Single stage impellers

Sebastian Maaß[a,*], Florian Metz[a], Torsten Rehm[b], Matthias Kraume[a]

[a] Technische Universität Berlin, Straße des 17. Juni 135, Sekr. MA 5-7, 10623 Berlin, Germany
[b] Vinnolit GmbH, 84489 Burghausen, Germany

ARTICLE INFO

Article history:
Received 8 March 2010
Received in revised form 3 June 2010
Accepted 5 June 2010

Keywords:
Drop size prediction
Slim reactors
Population balance equation
Liquid/liquid dispersion
Power input and baffling effect

ABSTRACT

Although investigations in the field of stirred liquid/liquid dispersions have a long history, new questions are still emerging in dealing with the different aspects of industrial applications, such as suspension polymerizations. In this study the influence of physical parameters on drop size and power consumption, like liquid level, stirrer speed, stirrer height and baffle length, were experimentally analyzed. The results were used to determine modeling approaches which are capable of displaying the influence of the named parameters. It was shown that the energy law ($d_p \sim \varepsilon^{-0.4}$; Shinnar, 1961 [1]) using the average energy dissipation only roughly predicts the Sauter mean diameter. The population balance equation (PBE) used with a one-zone modeling approach is slightly better in its prediction of results. Very satisfying predictions were obtained by using the PBE with a two-zone model. The overall deviations between calculated and predicted Sauter mean diameter was less than 10% using this approach. Only the successful prediction of the influence of the baffle length remained unattainable, even with the PBE two-zone model.

1. Introduction

Suspension polymerization is commonly used in the chemical industry for producing a wide variety of commercially important polymers, e.g. polystyrene, poly methylacrylate or poly vinyl chloride. In the initial phase of this polymerization the insoluble monomer is dispersed in an aqueous phase which contains a protective colloid or an inorganic suspension additive. This produces small liquid drops of monomer with a size range 1 μm to 3 mm. The drop size distribution (DSD) in this initial phase generally determines the final particle size distribution after the exothermic polymerization [2]. To control this distribution, a deeper understanding of the influencing parameters and an accurate prediction of the initial DSD is of major importance. Due to the economy of scale, reactor sizes are increasing. Only accurate models facilitate a precise scale-up for the reactor growth by increasing filling level.

In this study, an example production process of PVC is examined, with final mean diameters of solid particles ranging from 50 to 500 μm. PVC is one of the most important chemical products according to revenue. For example, the German PVC industry generates sales of 20 billion € per year. Eighty percent of PVC is produced by suspension polymerization worldwide. Growing markets and growing economies lead to higher PVC production rates. To achieve this more efficiently, newly built production reactors are increasing in height, while the diameter is fixed due to limits of space and issues of transportation. As a consequence, the ratio of liquid level height H vs. tank diameter T of such apparatus is enhanced; a ratio of 2.5 or higher is common and values of four are expected in the future. Predictive models for stirred vessels with a reactor height vs. diameter ratio of 1.0 are widely represented in the literature. The understanding of dispersion processes in slim reactors is incomplete and differs compared to the standard system and therefore extra difficulties are expected. Thus, the scale-up of a slim reactor from pilot plant to industrial scale remains a process where much empiricism, as well as expensive and time-consuming experimental programs, is usually required [3]. Only accurate predictions of system behavior will change this situation.

During the production process of PVC, stirring serves two purposes. Firstly, during the mixing of the organic phase of vinyl chloride with the aqueous phase, stirring facilitates effective dispersion. In the second step, stirring provides a homogeneous energy dissipation to control the agglomeration under polymerization and the cooling of the exothermic reaction.

In this work the task of dispersing two immiscible liquids was of major interest. In the experiments, the Sauter mean diameter ($d_{32} = \sum d_i^3 / \sum d_i^2$) and the DSD were analyzed. To predict these values the power numbers have been examined for various set-ups.

Abbreviations: CFD, computational fluid dynamics; DSD, drop size distribution; PBE, population balance equation; PVA, poly vinyl alcohol; PVC, poly vinyl chloride; RCI, retreat curve impeller.

* Corresponding author. Tel.: +49 30314 23171; fax: +49 30 314 21134.
E-mail address: sebastian.maass@tu-berlin.de (S. Maaß).

1385-8947/$ – see front matter © 2010 Elsevier B.V. All rights reserved.
doi:10.1016/j.cej.2010.06.007

Nomenclature

Nomenclature

a, b, c, C_i	numerical or prediction constants
d	stirrer diameter, drop diameter [m]
d_{32}	Sauter mean diameter [m]
d_{max}	maximum drop diameter [m]
h	bottom clearance, stirrer height [m]
H	liquid level [m]
l_B	baffle length [m]
n	stirrer speed [rpm]
M	moment [Nm]
N	number of drops [#]
Ne	power number
P	power [W]
Re	Reynolds number
t	time [s]
T	tank diameter [m]
w'^2	fluctuation velocity [m/s]
We	Weber number

Greek letters

γ	interfacial tension [mN/m]
ε	P/V—energy dissipation rate [W/m^3]
ε	P/M—energy dissipation rate [m^3/s^2]
η	dynamic viscosity [kg/(ms)]
λ	Kolmogoroff scale [m]
ν	kinematic viscosity [m^2/s]
ρ	density [kg/m^3]
σ	standard deviation
φ	dispersed phase fraction

The DSD were then simulated using empirical equations and the Population Balance Equation (PBE). The purpose of this work is to systematically compare experimental DSDs and Sauter diameters with predicted values for different set-ups of slim reactors.

2. State of the art: drop size prediction

2.1. Empirical and half empirical equations

In literature a great number of equations for drop size prediction are available. Most of them are based on the descriptions of Shinnar [1]. He explains that drop breakage is caused by micro-turbulences and that the emerging drops are about the same size as the micro-turbulence eddies [1]. These micro-turbulences were first described by Kolmogoroff [4] and are characterized by the micro scale λ (Kolmogoroff-Scale) which depends on the kinematic viscosity ν and the average energy dissipation rate ε:

$$\lambda = \left(\frac{\nu^3}{\varepsilon}\right)^{1/4} \tag{1}$$

This equation is based on estimations of the Sauter mean diameter d_{32} [4]. A key figure is the Weber number We which puts deforming forces in the agitated system in relation to the stabilizing interfacial energy:

$$\mathrm{We} = \frac{\rho n^2 d^3}{\gamma} \tag{2}$$

When the Weber number reaches a critical value, drop breakage occurs. With the average fluctuation velocity w' and the continuous phase density ρ, the critical Weber number is reached when interfacial tension γ equals the external deforming forces $\rho w'^2 d_{max}$. Under the assumption of constant energy input in the whole vessel and homogenous isotropic turbulences, the size of these micro-turbulences d_{max} can be calculated depending on the stirrer diameter d and We:

$$\frac{d_{max}}{d} = C_1 \left(\frac{n^2 d^3 \rho}{\gamma}\right)^{-3/5} = C_1 \mathrm{We}^{-0.6} \tag{3}$$

Because of the linear dependency between d_{max} and d_{32} [5], the equation for the Sauter mean diameter is presented in literature as the following:

$$\frac{d_{32}}{d} = C_1 C_2 \mathrm{We}^{-0.6} \tag{4}$$

The value of the constant C_1 depends on vessel geometry and the stirrer type, and has to be evaluated experimentally. In the literature the values for C_2 are between 0.38 and 0.7 [6]. Depending on the system, C_2 can be altered according to the following factor:

$$C_2 = C_4(1 + C_3\varphi), \tag{5}$$

with C_4 as a constant for the type of stirrer and C_3 reflecting the coalescence characteristic of the medium. The summarized equation also includes the volume phase fraction φ:

$$\frac{d_{32}}{d} = C_4(1 + C_3\varphi)\mathrm{We}^{-0.6} \tag{6}$$

Literature shows values for C_3 from 3 to 20 [7]. This equation assumes a linear correlation between φ and d_{32} that could not be confirmed by the experimental studies of Kraume et al. [8] and Angle et al. [9,10].

Furthermore, the validity of C_3 is questioned because of its interconnection with the drop size.

Eq. (3) with $\mathrm{We}^{-0.6}$ is also commonly expressed as a function of the specific power input with $\varepsilon^{-0.4}$. The Weber number is not affected by changes in the filling level and thus cannot effectively predict changes in the corresponding power input. Variations are introduced into the constant C_1 and need to be known. Therefore, the discussions about drop sizes in this study concerning the energy dissipation rate are always based on $C_1\varepsilon^{-0.4}$ and not on $C_1\mathrm{We}^{-0.6}$.

A broad and detailed overview of existing empirical and half empirical equations for the prediction of the Sauter mean diameter is given by Zerfa and Brooks [6] as well as by Angle and Hamza [10].

2.2. Population balance equations (PBE)

All presented drop size prediction equations assume an ideally mixed tank meaning the dependency on space is neglected. Such a simplification is too restrictive as the flow field, which highly influences drop breakage, coalescence, and the therefore the drop sizes, is usually very inhomogeneous throughout the stirred tank [11,12]. However, a detailed simulation using Computational Fluid Dynamics (CFD), which includes the coupled phenomena of the interactions of turbulent eddies in the flow field and the drops, requires great computational power and thus is very time consuming. A reliable compromise between detailed modeling and savings in computational time is offered by the compartment model approach. Various studies have shown promising improvements using a compartment model when compared to calculations using an average energy dissipation rate [13–16].

In this work the vessel is separated into two well-mixed regimes; one standing for the impeller region and the other for the remaining reactor volume. The size of these flow compartments is based on CFD simulations which were carried out using the software STAR-CCM+®. Furthermore, the unknown parameters such as the ratio of compartment volumes, energy dissipation rates and their exchange flow rates are computed. Those parameters are then implemented into a two-compartment model which calculates the drop size distributions for each regime based on the population

balance equation. Population balances have been extensively used in literature for the mathematical description of liquid/liquid processes in chemical engineering. In the PBE, the dispersed phase is expressed as a family of drops in which each individual is continuously created or destroyed, described by drop breakage or coalescence. For a batch reactor used in suspension polymerization, the convective terms are normally zero. The introduction of the two-compartment modeling now leads to transport terms between the two-zones within the batch vessel. The resulting equation can be described as follows:

$$V_{\text{zone},i}\frac{\partial N(d_\text{p})}{\partial t} = -D_\text{breakage} + B_\text{breakage} - D_\text{coalescence} + B_\text{coalescence} + \dot{V}_\text{in}N(d_\text{p}) - \dot{V}_\text{out}N(d_\text{p}) \quad (7)$$

The final two terms represent a change in the number of particles with different diameters d_p occurring over time. For the two birth terms (B_breakage, $B_\text{coalescence}$) and the two death terms (D_breakage, $D_\text{coalescence}$) many modeling approaches can be found within existing literature [see e.g. [17–21]].

2.3. Coalescence modeling

For modeling coalescence the frequently quoted model from Coulaloglou and Tavlarides [22] is employed for both breakage and coalescence kernels. The coalescence rate $F(d'_\text{p}, d''_\text{p})$ is assumed to be a two step process involving drop collision and film drainage of the continuous fluid. Thus it can be expressed as the product of the collision frequency $h(d'_\text{p}, d''_\text{p})$ and the coalescence efficiency $\lambda(d'_\text{p}, d''_\text{p})$. The collision frequency from Coulaloglou and Tavlarides [22] has found broad acceptance in the scientific community and is formulated as shown in Eq. (8).

$$h(d'_\text{p}, d''_\text{p}) = c_{1,\text{coal}}\frac{\varepsilon^{1/3}}{1+\varphi_\text{d}}(d'_\text{p}+d''_\text{p})^2(d'^{2/3}_\text{p}+d''^{2/3}_\text{p})^{1/2} \quad (8)$$

Liao and Lucas [21] give a broad and updated overview of research in the field of coalescence efficiencies. They differentiate between three model approaches which have been used for the calculation of coalescence efficiency: the energy model, critical approach velocity model and film drainage model. Although the validity of the film drainage model has been criticized, it remains the most popular approach and forms the starting point of almost all subsequent models, including that developed by Coulaloglou and Tavlarides [22], given in Eq. (9).

$$\lambda(d'_\text{p}, d''_\text{p}) = \exp\left(-c_{2,\text{coal.}}\frac{\eta_\text{c}\rho_\text{c}\varepsilon}{\gamma^2(1+\varphi_\text{d})^3}\left(\frac{d'_\text{p}d''_p}{d'_\text{p}+d''_\text{p}}\right)^4\right) \quad (9)$$

Their entire coalescence rate $F(d'_\text{p}, d''_\text{p})$ gives low values for the contact of two small or two large drops and high values for the contact of a small and a large drop. The influence of surfactants in this coalescence model is only expressed by the surface tension γ within the coalescence efficiency (see Eqs. (8) and (9)). This overlooks the fact that contaminants such as surfactants are modifying the drop surfaces and hence reducing the film drainage. Moreover, the concept of a concentration threshold above which coalescence is drastically reduced is already well established in empirical models and remains central when modeling the effect of DSDs in liquid–liquid systems [23]. Although the number of published models is extremely high, no approach for the PBE of the drainage model takes this interrelation into account.

2.4. Breakage modeling

The number of models published about the breakage process is even higher than those regarding coalescence. The most significant have been recently analyzed by Liao and Lucas [19]. In many cases the different authors assume that drop breakage occurs due to drop-eddy collisions. The most widely used and quoted model for the drop breakage rate is the approach of Coulaloglou and Tavlarides [22] given in Eq. (10).

$$g(d_\text{p}) = c_{1,\text{break.}}\frac{\varepsilon^{1/3}}{(1+\varphi_\text{d})d_\text{p}^{2/3}}\exp\left(-c_{2,\text{break.}}\frac{\gamma(1+\varphi_\text{d})^2}{\rho\varepsilon^{2/3}d_\text{p}^{5/3}}\right) \quad (10)$$

This breakage rate has a maximum for a certain critical particle diameter. This has been generally criticized by Baptat et al. [24]. The intention of Coulaloglou and Tavlarides [22] is to use the breakage time in order to determine the breakage rate. The mentioned maximum with increasing mother drop diameter occurs because the duration of breakage increases with rising diameter. Therefore, once the diameter has reached a certain size the breakage rate is affected by the breakage time and decreases. In combination with the breakage rate, the number of daughter drops ν and the daughter drop size distribution $\beta(d_\text{p})$ have to be formulated. Experimental results have shown that the most probable event for the number of daughter drops is a binary breakage event [25,26], and therefore ν was set to a value of two. Further assumptions are made about the binary coalescence, which remains common, and the Gaussian daughter drop size distribution [22].

The commercial software PARSIVAL® (Particle Size Evaluation) was used as the population balance solver [27]. This is a powerful tool which uses an adaptive Galerkin *h–p* method for the discretization of time and drop size. Our own experimental data were used for the parameter estimation of the numerical parameters in the PBE. The confidence interval of the fitted parameters needed to be small compared to the value of the parameter, and had to remain independent from one another.

In liquid/liquid dispersions the final DSD is dependent on the equilibrium between drop breakage and coalescence rates. Thus, for the same operating conditions, the final DSD should be independent of the initial DSD used in any PBE-solver. Therefore, a sensitivity analysis with PARSIVAL® was carried out using Gaussian and log-Gaussian distributions with varying Sauter mean diameters from 3×10^2 to 5×10^4 μm. After 1 min of real time, no dependency on the initial distribution could be found, i.e. the DSD converged all to the same final state. The calculation time for the first minute increased with the Sauter mean diameter, especially for the parameter optimization. A Gaussian distribution with a d_{32} of 870 μm was used for all simulations.

3. Material and methods

In order to investigate the influence of different geometry and process parameters on the drop size distribution in liquid/liquid systems, various experiments were carried out.

3.1. Experimental set-up

A model system (n-butyl chloride from Merck with deionized water) was used at a dispersed phase fraction of 45 or 25% in water at atmospheric pressure and a constant temperature of 20 °C. Coalescence was reduced by a poly vinyl alcohol (PVA) provided by Vinnolit GmbH & Co. KG. PVA was mainly used at a concentration of 1000 ppm (mass PVA/mass n-butyl chloride). This decreased the interfacial tension between water and n-butyl chloride from 37.1 mN/m [28] to 5 mN/m. The stirrer speed was varied from 250 to 700 rpm for different reactor heights and baffle immersion depths (l_B). Furthermore, different stirrer and baffle types were investigated. The tank diameter T was 155 mm and the bottom clearance h of the stirrer was kept constant at $0.15T$ for the retreat curve impellers (RCI) and $h = 1.1T$ for the used blade impeller (see also

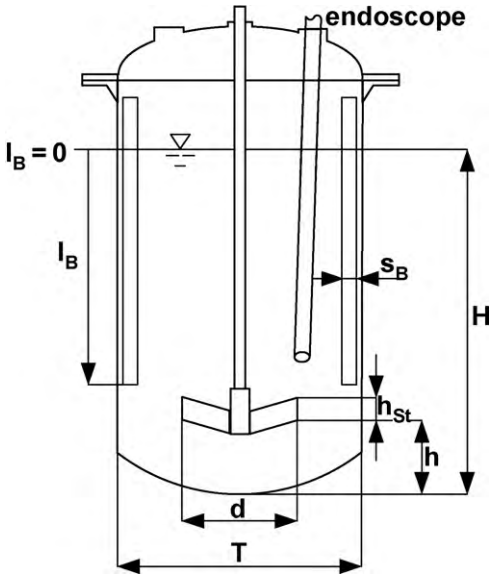

Fig. 1. Experimental set-up and dimensions of the used stirred tank.

Fig. 1 and Table 2). The volume of the system for the most frequently used application ($H/T = 2.15$) is around six liters. An overview of the measurement program for the analysis of the drop sizes is given in Table 1.

3.2. Measurement procedure

The measurements of the power number were carried out in the same vessel as a single phase system using pure deionized water. Here the stirrers were attached to a viscometer to measure the torque and rotational frequency. Using these two figures, the agitation power P and the power number Ne can be calculated:

$$\mathrm{Ne} = \frac{2\pi M}{\rho n^2 d^5} = \frac{P}{\rho n^3 d^5} \tag{11}$$

These analyses were carried out at different rotational speeds. By increasing stirrer Reynolds number ($\mathrm{Re} = \rho n d^2/\eta$), the power number decreases and then becomes constant in the turbulent area of a stirrer Reynolds' number >10^4 [29]. Measurements for all parameter configurations were carried out five times with an average standard deviation of less than 1%. For the analysis of the drop sizes a special in situ endoscope technique was used [30]. Using this technique, drop size distributions for all phase fractions, even under transient conditions, can be determined with high time resolution. The drop size distribution was found independent of local position due to the high volume streams within the vessel, as opposed to gas/liquid systems analyzed by Laakkonen et al. [31]. The high volume streams ensure the same drop size distribution at every place in the vessel. This has already been proven by Ritter and Kraume [32] for strong coalescing systems but only at a H/T ratio of 1.0 [32].

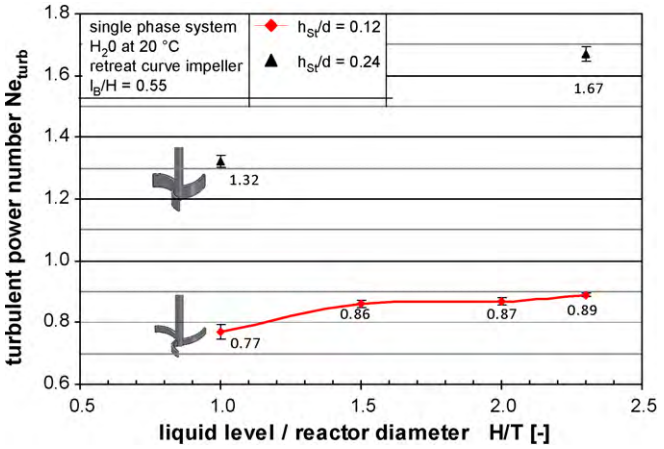

Fig. 2. Turbulent power number for different H/T ratios for two different retreat curve impellers.

4. Results and discussions

It has long been recognized that some of the important factors which influence the DSD in a suspension polymerization are geometry of the vessel, size of the vessel, type of stirrer, presence of baffles, and the amount of energy supplied to the system by the impeller. While all these parameters are underrepresented within popular models, it is the major interest of this work to focus experimental and numerical investigations on these parameters.

4.1. Power number

It is necessary to know the exact power consumption of a given system set-up in order to predict the DSD and the Sauter mean diameter using PBE or empirical correlations. The power consumption of the two RCIs was determined at various liquid levels. Both had a diameter d of 0.4T, and the height of the stirrers h_{St} was varied between $h_{St}/d = 0.12$ and 0.24. For the flatter stirrer of the two, the influence of the baffle length (l_B) and baffle type (cylindrical and blade) was also investigated at a fixed H/T ratio of 2.15.

Fig. 2 shows the development of the turbulent power numbers at different H/T ratios; which remains constant for $\mathrm{Re} > 10^4$. For both stirrers, the power number increases with rising H/T. This means more power is consumed at larger filling levels when set at a constant stirrer speed and reactor diameter. The increase in power consumption is not proportional to the rise in the reactor volume. A doubling in mass leads to an increase of only 13% in power consumption. The increase is stronger in lower rather than higher liquid levels. This means that at a certain distance from the impeller to the liquid surface, the power uptake does not increase any further, even if the liquid level is increased. These results are in agreement with those of Nocentini et al. [33] who found almost no effect of liquid height on the power number for a multiple impeller system with four stirrers.

Interestingly, the doubling of the stirrer height does not lead to a doubling in the power number. It increases only by a factor of 1.72

Table 1
Overview of the measurement program analyzing the liquid/liquid system.

H/T	V_R [L]	Stirrer type	n [rpm]	l_B/H	c_{PVA} [mg/g]	φ_{disp}
1.00	2.711	RCI ($h_{St}/d = 0.12$; 0.24)	400, 250	0.55	1	0.45
1.40	4.026	Blade impeller ($h_{St}/d = 0.06$)	410	1.00	0.1	0.25
1.50	4.185	RCI ($h_{St}/d = 0.12$)	400, 550	0.55	1	0.45
2.00	5.650	RCI ($h_{St}/d = 0.12$)	400, 600	0.55	1	0.45
2.15	6.015	RCI ($h_{St}/d = 0.12$; 0.24)	400, 250, 325, 700	0.10–0.80	1	0.45
2.30	6.496	RCI ($h_{St}/d = 0.12$)	400	0.55	1	0.45

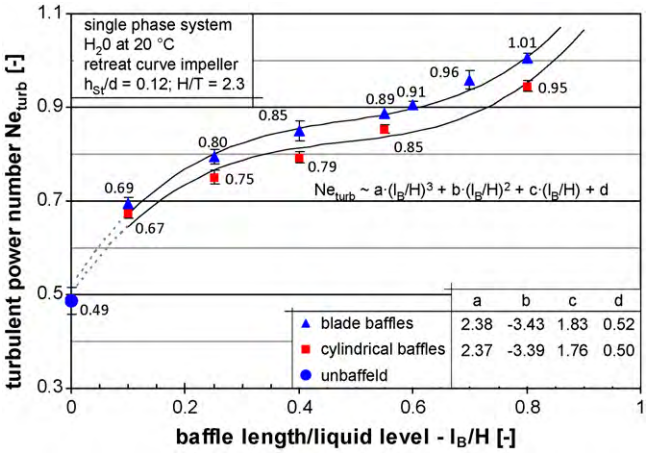

Fig. 3. Turbulent power numbers for two kinds of baffles over different heights of immersion of the baffles measured with a retreat curve impeller ($h_{St}/d = 0.12$).

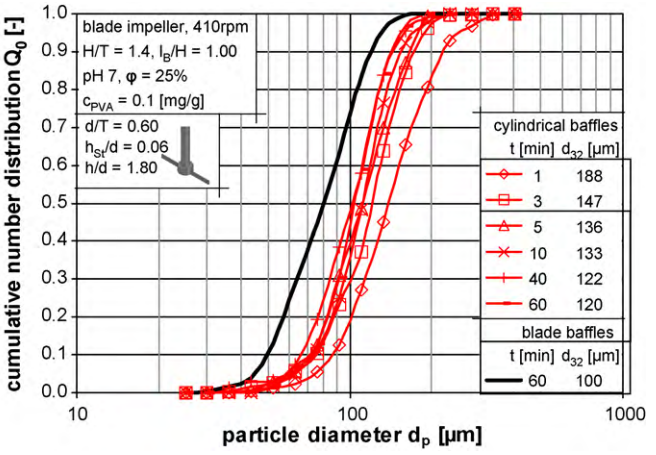

Fig. 4. Transient development of the cumulative number distribution for a constant stirrer speed of 410 rpm using a blade stirrer and cylindrical baffles and comparison of the 60 min distribution resulting for constant system parameters with cylindrical and blade baffles.

for the H/T ratio of 1.0 and by a factor of 1.88 for the H/T ratio of 2.3.

The influence of the baffle length has been seldom discussed in the literature. Karcz and Major [34] have presented the influence of baffle length within the following systems; standard radial impellers, Rushton and Smith turbine, standard axial impeller, pitched blade turbine and propeller. They have investigated a vessel with four planar baffles and H/T ratio of 1.0 [34]. These investigations revealed a strong relationship between baffle length and power consumption. This has interesting implications for suspension polymerization processes in terms of potential energy savings. No results of the influence of baffle immersion height on power consumption in slim reactors have been found in the existing literature. For that reason, different aspects of the baffling effect have been investigated in detail. All measurements have been carried out five times with an average standard deviation of less than 1%. Additionally, the absolute values of the turbulent power numbers for the large baffle lengths are in good agreement with those of Li et al. [35], who determined turbulent power numbers experimentally and with CFD calculations in the range of 1.0 for a vessel with one baffle ($l_B = H$).

Vessels for industrial applications are often equipped with cylindrical baffles in order to simplify cleaning. These have a slightly different influence on the flow field than the "standard" planar blade baffles. In Fig. 3, the power numbers for both kinds of baffles are compared for different immersion depths. Less tearing edges of the cylindrical baffles obviously consume less power than the blade baffles. Both series of experimentally obtained values show the same pattern. Starting with no baffles and increasing the immersion depth to 25% of the liquid level in the vessel, the power consumption is increased by 53% for the cylindrical and even 63% for the blade baffles. Towards higher immersion depths, the slope of both curves decreases and reaches its minimum between baffle lengths of 40 and 55%. Between these two points, the power number grows from 0.85 to 0.89 for the blade baffles and from 0.79 to 0.85 for the cylindrical baffles. Towards higher immersion depths, the increase of Ne over baffle length again leads to a stronger growing power consumption. Such results with sigmoidal behavior have been reported in literature for single Rushton turbines [34] as well as dual Rushton turbines [36]. The results of this study have been approximated for both types of baffles with a cubic equation:

$$\mathrm{Ne}_{\mathrm{turb}} \approx a\left(\frac{l_B}{H}\right)^3 + b\left(\frac{l_B}{H}\right)^2 + c\left(\frac{l_B}{H}\right) + d \qquad (12)$$

The values for the parameters of this polynomial are given in the table of Fig. 3. Based on Eq. (11), it is possible to calculate the energy dissipation rate for a certain geometrical set-up, which is of major importance for the prediction of DSD and the Sauter mean diameter with the PBE or empirical correlations.

4.2. Drop sizes

The transient evolution of the drop sizes for different impeller speeds, geometrical set-ups and stirrer types have been investigated at certain points in time (1, 3, 5, 10, 15, 25, 40 and 60 min). The DSD were determined experimentally and the Sauter mean diameters were calculated from the measured distributions ($d_{32} = \sum d_i^3 / \sum d_i^2$). These data sets give a broad base for evaluating the different models from the literature. The sensitivity of single numerical parameters within certain drop size prediction approaches can also be determined.

The first results show a difference in the DSD for cylindrical and blade baffles. They have been obtained with a single blade impeller at a constant stirrer speed of 410 rpm and a liquid level of 1.4T (Fig. 4). As expected, the drops become smaller the longer the duration of stirring. It is worth emphasizing that a differentiation between the 5, 10, 40 and 60 min distribution can only be done with the comparison of the resulting d_{32}. The size change within the first 5 min is the strongest. These values are included within the table in Fig. 4. The transient drop sizes have been recorded with the same parameter set but using blade baffles instead of cylindrical ones. For an easier comparison, only the Sauter mean diameter and the cumulative number distribution for the blade baffles after 60 min are given (see also Fig. 3—influence of the baffle type on the power number). The blade baffles with higher values for Ne in the turbulent regime lead to smaller drops. The resulting difference in Sauter mean diameter almost reaches 20%. This strong influence of the energy dissipation rate on the drop sizes was not expected.

Many investigations have been carried out, using a retreat curve impeller, because it is the traditional impeller in PVC production processes and is still used in numerous industrial applications in that field. Therefore, a focus on this specific impeller was set in the following investigations. The given geometrical dimensions in Table 2 reflect those traditional standards and have been the settings for all following experiments of this series.

Table 2
Dimensions of the used stirred tank.

T	H	l_B	s_B	h	d
155 mm	2.3T	0.1–1.0H	0.08T	0.15T	0.55T

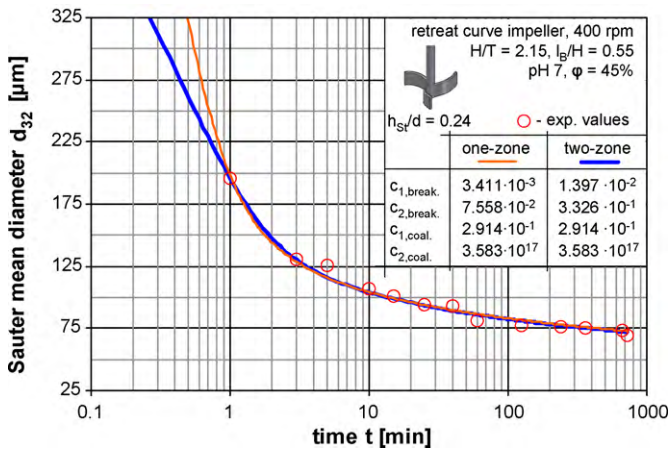

Fig. 5. Transient Sauter mean diameter d_{32} with a RCI ($h_{St}/d = 0.24$) and simulation results with optimized numerical parameters for a one- and a two-zone model.

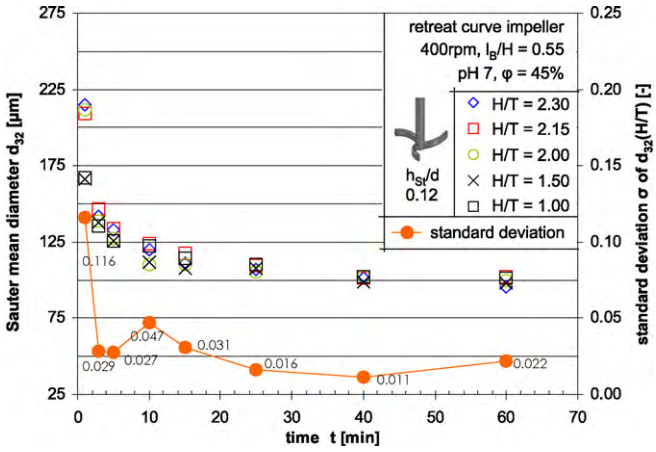

Fig. 6. Transient Sauter mean diameter d_{32} with the standard RCI ($h_{St}/d = 0.12$) and the resulting standard deviations of the different $d_{32}(H/T)$ at specific points in time are shown.

As already mentioned, a parameter fitting is necessary for the precise drop size prediction. Even the use of the energy law ($d_{32} \sim \varepsilon^{-0.4}$) after Shinnar [1] needs a single parameter adaptation. One specific system set-up was used to determine all necessary parameters. The details of this set-up are given in Fig. 5. The used PBE model for the transient simulations was the one presented by Coulaloglou and Tavlarides [22]. As mentioned previously, a large number of different PBE models with the purpose of predicting drop size have been presented. For the same experimental set-up, different approaches can be applied because most of them show good agreement between prediction and experimental data [37]. The model approach by Coulaloglou and Tavlarides [22] has been selected because of its unique simplicity that made it a standard in population balance modeling.

As the prediction quality of a PBE model improves, the transient behavior represented in the model becomes better. This is especially true of the breakage parameters, which need to be identified with great care. Therefore, one single experiment was carried out during 12 h. The experimental results for the Sauter mean diameter at different points in time are given in Fig. 5. The four parameters ($c_{1,break.}$, $c_{2,break.}$, $c_{1,coal.}$, $c_{2,coal.}$) have been estimated for the one- and the two-zone model approach. The simulation results and the final parameters are also given in Fig. 5. It is interesting to see that d_{32} of the coalescence hindered system still decreases after 720 min of uninterrupted stirring. It may be noticed that the change in the first 5 min is l.5 times larger than its decrease during the remaining duration of 715 min. Because the average production process takes place within 60 min, all following experiments were reduced to this value. The parameter identification for the energy law was carried out based on the experimental d_{32} after 60 min of stirring. With the assumptions of a pure linear relation between d_{32} and d_{max} [5] and no further influence of other variables, the constant was determined to the value of 8.72. This result is in good agreement with the results from literature already cited in this study. All following experimental results (variation of H/T; stirrer speed and l_B/H) can now be compared with the drop size prediction based on the filled parameters summarized in Table 3.

These first results give a clear direction for the following investigations. Small changes in the geometrical parameters like the baffle type have a major influence on the DSD. They can be identified easily by comparison of the transient Sauter mean diameters.

The prediction of this behavior needed precise parameter fitting for all approaches. Therefore, they have been defined in a long time experiment to minimize errors. Their values are given in Table 3. They were kept constant for all following simulations using the one- or the two-zone model.

4.3. Influence of liquid level/vessel diameter ratio on drop sizes

The standard liquid level in academic studies is equal to the vessel diameter, which is very rare in industrial applications. The number of industrial applications with filling levels of more than twice the vessel diameter is growing extensively. Therefore, the influence of the H/T ratio on the drop sizes was investigated. The resulting transient Sauter mean diameters are presented in Fig. 6.

Interestingly, the drop sizes over time are nearly independent from the H/T ratio. Only during the first minute, the larger reactor volumes of $H/T = 2.0$; 2.15 and 2.3 show higher values of d_{32}. This is also illustrated by the resulting standard deviation (σ) of those Sauter mean diameters which is presented on the second ordinate in Fig. 6. The average diameters from the five different H/T ratios are calculated together with the resulting standard deviation. The value of the standard deviation after the first minute is four times larger than the average value of all other standard deviations for the rest of the experiment. This reflects a strong deviation in the beginning of the mixing process which disappears within less than 10 min. After 60 min of stirring, no significant difference between all five set-ups could be found which implies an independency of d_{32} on the reactor volume for a constant stirrer speed and hence a dependency of d_{32} on the stirrer tip speed ($w_{Tip} = 2\pi nd$) rather than on ε.

The dependency of the Sauter mean diameter on the energy dissipation rate after 60 min of stirring is shown in Fig. 7. In this plot, the results for different H/T ratios are supplemented with those for different stirrer speeds and heights (h_{St}). The filled diamonds are the results of d_{32} for different H/T ratios at a constant stirrer speed of 400 rpm. All set-ups show a d_{32} around 100 µm. These values are in agreement with the experimental results of Zerfa and Brooks [6].

Table 3
Parameter overview.

Model approach	C_1	$c_{1,break.}$	$c_{2,break.}$	$c_{1,coal.}$	$c_{2,coal.}$
$d_{32}/d_{max} = C_1\varepsilon^{-0.4}$	8.72	–	–	–	–
PBE with one-zone model	–	3.411×10^{-3}	7.558×10^{-2}	2.914×10^{-1}	3.583×10^{17}
PBE with two-zone model	–	1.397×10^{-2}	3.326×10^{-1}	2.914×10^{-1}	3.583×10^{17}

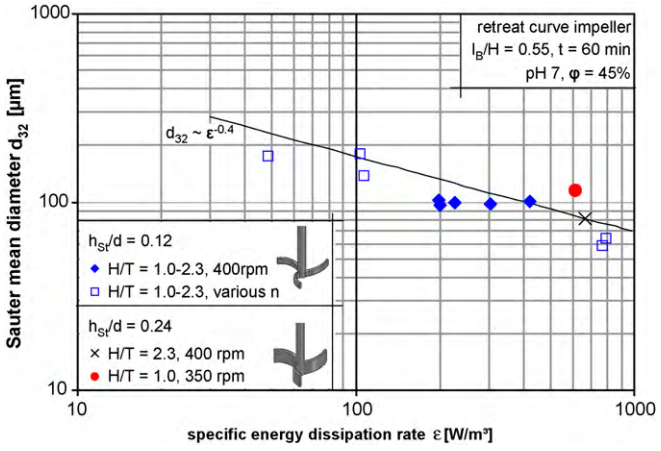

Fig. 7. Dependency of the Sauter mean diameter d_{32} on the specific energy dissipation rate ε for various system characteristics, always after 60 min of mixing.

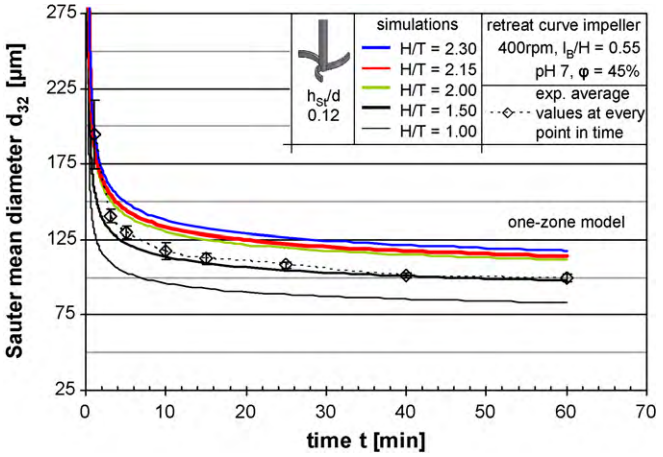

Fig. 8. Simulation results of the transient Sauter mean diameter with the standard RCI ($h_{St}/d = 0.12$) for various H/T. The results were achieved with a one-zone model and are compared with averaged experimental values shown in Fig. 6.

Compared with the results for the power number in Fig. 2, doubling the vessel content leads to an increase in power consumption by only 15%. This can also be interpreted as a decrease in specific energy dissipation rate for obtaining the same. With 13% more energy (see Fig. 2 for the increase of Ne over H/T) the product volume can be increased by a factor of 2.3 (by increasing the H/T ratio up to 2.3). This behavior could not be predicted with the proportionality between d_{32} and ε. The influence of the stirrer speed for the different set-ups, represented by the open squares, is much more significant for ε than the influence of the reactor volume (see Eq. (11)). The general dependency of the Sauter mean diameter from the stirrer speed is still reflected in a good accuracy using $d_{32} \sim \varepsilon^{-0.4}$ after Shinnar [1].

The dependency on w_{Tip} is also disproved by the use of similar-shaped RCIs with different impeller heights. A Sauter mean diameter of around 100 μm is produced with standard RCI ($h_{St} = 0.12$) at $H/T = 2.15$. The doubling of the stirrer height is not affecting the tip speed of the stirrer for a constant n (400 rpm) but the Sauter mean diameter is nearly 80 μm (black cross in Fig. 7). This means for constant w_{Tip} the increase of the stirrer height leads to a decrease in drop sizes. This observation of increasing impeller power number with increasing impeller height is expected [38], and is also shown in Fig. 2. The power number increases from 0.89 to 1.67, correlated with the energy law $(d_{32} \sim \varepsilon^{-0.4}) \rightarrow (1.67/0.89)^{-0.4} = 0.77$. The experimental results are in good agreement with the theoretical correlation. Naseef et al. [38] reported about a proportionality between d_{32} and h_{St}. They found a potential proportionality with exponents between −0.24 and −0.5 depending on the stirrer speed; lower speeds led to lower exponents in their studies. The exponent identified in this study is −0.32. Similar results have been achieved by Sechremeli et al. [39], who compared a disk and a blade impeller at the same tip speed but with the same impeller height at $H/T = 1.0$ and low dispersed phase fractions ($\varphi \leq 0.1$).

The predictive capabilities of the one- and the two-zone model are demonstrated by a direct comparison of experimental and simulation results for different H/T ratios in Figs. 8 and 9. Both model approaches are using the same physical and geometrical parameters. The numerical constants are the presented ones in Fig. 5 and were kept constant for all simulations throughout the whole study. The calculation time for 60 min process time, using a single standard CPU, was 15 min for the one-zone model and 25 min for the two-zone model.

Because of the independency of the d_{32} on the liquid level for a constant stirrer speed, the experimental results for the different H/T ratios are presented as the average Sauter mean diameter with the standard deviation at certain point in time. In Fig. 8 the direct comparison with the simulation results of the one-zone model are given. Only one curve ($H/T = 1.50$) fits the experimental results. The drop sizes for $H/T = 1.00$ are much smaller than the experimental results, according to the higher energy dissipation rate P/V for a smaller volume. The behavior for the larger H/T ratios is opposite to this. It is not possible to predict the system behavior precisely using the PBE with the one-zone model. A completely different situation for the simulation results is achieved with the two-zone modeling. Fig. 9 shows this clearly, especially after 10 min of mixing, all simulations for all H/T ratios result in almost the same Sauter mean diameters. This reflects the experimental data very well.

To evaluate the quality of d_{32} prediction using the PBE with the two-zone model, not only the stirrer (RCI with $h_{St} = 0.12$ and 0.24) and the geometrical set-up was changed (H/T) but also the stirrer speed was varied from 250 to 700 rpm. The results are given in Fig. 10. For a better judgment of the deviation between experimental and simulation results in the beginning of the mixing process, the data are presented in a semi-logarithmic diagram. Fortunately the simulations are also predicting the transient Sauter mean diameter behavior for different stirrer speeds very well, except the results for 250 rpm. Here the experimental values are much smaller than the simulation results. It has to be mentioned that 250 rpm is lower than the minimum stirrer speed, which is necessary for a

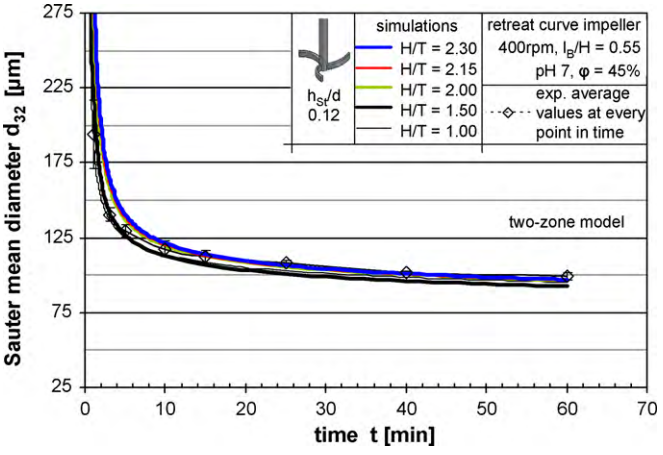

Fig. 9. Simulation results of the transient Sauter mean diameter with the standard RCI ($h_{St}/d = 0.12$) for various H/T. The results were achieved with a two-zone model and are compared with averaged experimental values shown in Fig. 6.

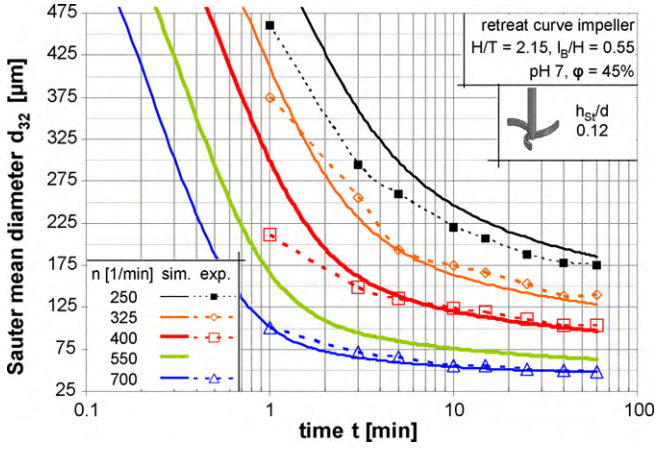

Fig. 10. Simulation results of the transient Sauter mean diameter with the standard RCI ($h_{St}/d = 0.12$) at $H/T = 2.15$ for various stirrer speeds. The results were achieved with a two-zone model and are compared with experimental values.

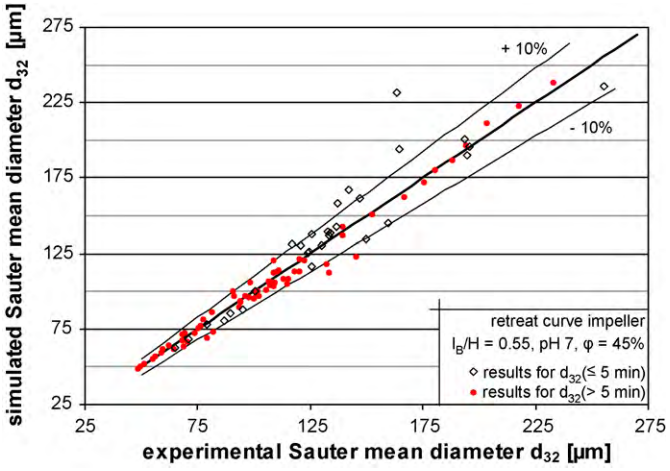

Fig. 12. Deviation of experimentally achieved d_{32} and predicted mean diameters with the two-zone PBE simulations at different stirrer speeds, H/T ratios (1.0–2.3) and with different retreat curve impellers ($h_{St} = 0.12$ and 0.24).

full mixed dispersion. Even after 60 min of stirring almost 20% of the organic phase still needed to be dispersed. That leads to two important influence factors. Firstly, the concentration of the PVA for the rest of the n-butyl chloride is 20% higher. That leads to smaller drops in the mixed part of the reactor. Secondly, the dispersed phase fraction in the mixed part is not 45 but 40%, causing smaller droplets in the measurement zone. Both influence parameters, the higher colloid concentration and the lower dispersed phase fraction, have been mentioned by Zerfa and Brooks [6] as crucial parameters which decrease the drop size. This behavior could not be predicted using the PBE, because minimum stirrer speed is a pre-condition in this modeling approach.

All three introduced drop prediction approaches are compared in Fig. 11. This is a parity plot for the Sauter mean diameters after 60 min of mixing. Both RCIs ($h_{St} = 0.12$ and 0.24), all different H/T ratios (1.0–2.3) and all stirrer speeds larger than the minimum necessary are presented. The deviations of ±10 and 30% are also plotted. This illustration makes it obvious, that the PBE using the two-zone model approach is highly precise and better than the other prediction methods. Nearly all predicted Sauter mean diameters have deviations smaller than 10%. The PBE with the energy averaged one-zone model reaches deviations smaller than 20% and the widely used simplification of the energy law ($d_{32} \sim \varepsilon_{average}^{-0.4}$) leads to deviations larger than 30%.

A more detailed look on the accuracy of the prediction of d_{32} using the PBE with the two-zone model is made in Fig. 12. All transient Sauter mean diameters for all varied parameters (H/T, n and different h_{St}) are compared with the predicted values. The open diamonds represent the values of the transient Sauter mean diameter for 5 min or less minutes of mixing, the filled dots present the Sauter mean diameters after more than 5 min of mixing. All larger deviations occur only within the first 5 min.

The population balance equation regarding the inhomogeneity of stirred tanks using the two-zone model approach predicts Sauter mean diameters for a broad variation of system parameters after one careful parameter fitting. It is possible to simulate the change of the stirrer height, liquid level, and stirrer speed with the two-zone model approach.

4.4. Baffling effect on drop sizes

The last investigated parameter influencing the drop size in this study is the immersion depth of the two baffles. Nine different depths of blade baffles have been investigated for a constant stirrer speed (400 rpm) and H/T ratio (2.15) over 60 min of mixing. The transient Sauter mean diameters are given over the baffle length vs. liquid level ratio in Fig. 13. The d_{32} results are clearly divided into

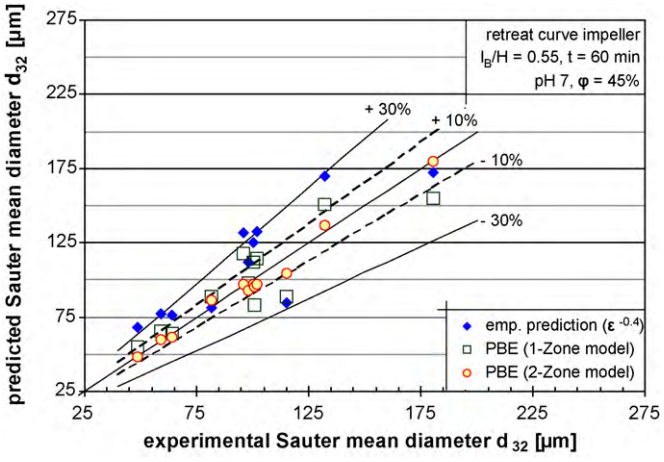

Fig. 11. Deviation of experimentally achieved d_{32} and three different drop size prediction methods after 60 min mixing at different stirrer speeds, different H/T (1.0–2.3) and with different retreat curve impellers ($h_{St} = 0.12$ and 0.24).

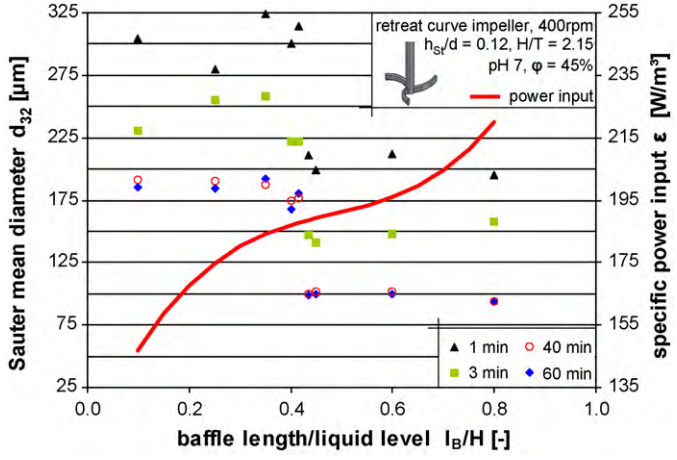

Fig. 13. Influence of the baffle length on the transient Sauter mean diameter d_{32} for constant stirrer speed (400 rpm) and constant $H/T = 2.15$ compared with the corresponding specific power input.

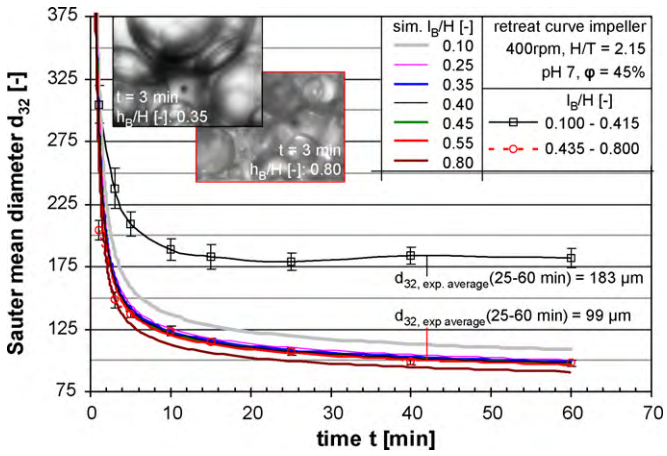

Fig. 14. Comparison of experimental and simulation results of transient d_{32} for various baffles immersion depths at a constant stirrer speed (400 rpm) and $H/T = 2.15$.

two different regimes—under and above a certain height of immersion. This differentiation is obvious for all four presented terms.

The value after 1 min is around 300 μm for the lower and 200 μm for the larger immersion depths. The same differences can be found for the results at the time point after 3 min (230–150 μm), after 40 min (180–100 μm) and also after 60 min (180–100 μm) of stirring. The fluctuation of the measured values is higher in the beginning of the process due to the sensitivity of the d_{32} to single large drops, which occur in the first 3 min. They achieve a standard deviation over all immersion depths between 4 and 7%. For longer operating time (≥5 min), standard deviations between 1 and 4% have been achieved. Therefore, it is much more accurate to discuss the 40 or 60 min results which show the leap between $l_B/H = 0.415$ and $l_B/H = 0.435$. Lower l_B/H ratios than 0.415 led to d_{32}(60 min) of around 180 μm and higher l_B/H ratios than 0.435 led to d_{32}(60 min) of around 100 μm. This behavior was really surprising to the authors. Therefore the specific power input has been introduced via the second ordinate of Fig. 13. The specific power input follows the same behavior as the power numbers presented in Fig. 3. Surprisingly both (ε and Ne) show the lowest changes in the region where the drop size leap (l_B/H between 0.35 and 0.55) occurs. A tentative prediction of this behavior using the PBE with the two-zone model and two example images for both l_B/H-regions are shown in Fig. 14.

The direct comparison of the experimental and the simulation results show that the experimentally determined leap in the development of d_{32} of l_B/H could not be reproduced with the population balance equation. A slight change to smaller drops with smaller immersion depths only reflects the change in the power number or power input. The reason for this failure could be a poor reflection of the flow field through the two-zone model. The CFD calculations for the determination of the compartment volume ratio, ratio of energy dissipation rates and their exchange flow rates have only been carried out for ones of a constant $l_B/H = 0.55$ ratio. It seems to be necessary to analyze the influence of l_B on the flow field experimentally and also with CFD simulations. This should help to understand the dramatic change of d_{32} at an immersion depth of the baffles around 0.43—we expect a dramatic change in the flow pattern at this point.

5. Conclusion and outlook

To analyze the influence of physical parameters in slim reactors, comparable experiments were carried out. Those results were used to determine modeling approaches which are capable of displaying the influence of parameters like liquid level, stirrer speed, stirrer height and baffle length. It was shown that the energy law using the average energy dissipation rate predicts only roughly the Sauter mean diameter. The PBE using a one-zone modeling approach is only a little better in its prediction results. Very satisfying results were achieved using the PBE with a two-zone model. The overall deviations between calculated and predicted Sauter mean diameters were less than 10%. Only the prediction of the influence of the baffle length was unacceptable even with the PBE two-zone model.

The reason for this is the lack of knowledge about the influence of this parameter on the flow field and the local energy dissipation rates. Such a change in the geometrical set-up is not covered with a single flow field simulation, carried out in this study. Therefore, intense flow field analysis will be carried out in the future. A direct coupling between CFD and PBE would avoid such errors but also increase the computational costs. A promising alternative approach to avoid the high computational costs for the solution of the coupled system could be to apply the direct quadrature method of moments for the solution of the population balance equation [40]. In conclusion, the prediction of drop sizes is of major interest for many industrial applications. To increase the accuracy of such calculations a detailed knowledge of the flow field is necessary. If this knowledge is already available the PBE-zonal-model approach is a very powerful tool to describe the transient drop sizes in stirred liquid/liquid dispersions.

All investigations have been carried out in a stirred tank with a maximum liquid level height to vessel diameter ratio of 2.3. Industrial applications have already reached H/T ratios of 5.0. Obviously single stage stirrers will not be able to disperse immiscible fluids in such settings. Therefore analysis of multi-stage stirrers in slim reactors with H/T ratios of 5.0 has to be carried out. Those results will be presented in part two of this study.

Acknowledgement

The authors gratefully acknowledge Ms. So-Jin Kim for performing the baffling effect experiments.

References

[1] R. Shinnar, On the behaviour of liquid dispersions in mixing vessels, J. Fluid Mech. 10 (1961) 259–275.
[2] A.H. Alexopoulos, C. Kiparissides, On the prediction of internal particle morphology in suspension polymerization of vinyl chloride. Part I: the effect of primary particle size distribution, Chem. Eng. Sci. 62 (2007) 3970–3983.
[3] E. Vivaldo-Lima, P.E. Wood, A.E. Hamielec, A. Penlidis, An updated review on suspension polymerization, Ind. Eng. Chem. Res. 36 (1997) 939–965.
[4] A.N. Kolmogoroff, Local structure of turbulence in an incompressible viscous fluid at very high Reynolds numbers, Dokl. Akad. Nauk. SSSR 30 (1941) 299–303.
[5] F.B. Sprow, Drop size distributions in strongly coalescing agitated liquid–liquid systems, AIChE J. 13 (1967) 995–998.
[6] M. Zerfa, B.W. Brooks, Prediction of vinyl chloride drop sizes in stabilised liquid–liquid agitated dispersion, Chem. Eng. Sci. 51 (1996) 3223–3233.
[7] A.W. Pacek, S. Chamsart, A.W. Nienow, A. Bakker, The influence of impeller type on mean drop size and drop size distribution in an agitated vessel, Chem. Eng. Sci. 54 (1999) 4211–4222.
[8] M. Kraume, A. Gäbler, K. Schulze, Influence of physical properties on drop size distributions of stirred liquid–liquid dispersions, Chem. Eng. Technol. 27 (2004) 330–334.
[9] C.W. Angle, T. Dabros, H.A. Hamza, Predicting sizes of toluene-diluted heavy oil emulsions in turbulent flow. Part 1—application of two adsorption kinetic models for σ^E in two size predictive models, Chem. Eng. Sci. 61 (2006) 7309–7324.
[10] C.W. Angle, H.A. Hamza, Predicting the sizes of toluene-diluted heavy oil emulsions in turbulent flow—Part 2: Hinze–Kolmogorov based model adapted for increased oil fractions and energy dissipation in a stirred tank, Chem. Eng. Sci. 61 (2006) 7325–7335.
[11] S. Schmelter, Modeling, analysis, and numerical solution of stirred liquid–liquid dispersions, Comp. Methods Appl. Mech. Eng. 197 (2008) 4125–4131.
[12] S. Kresta, Turbulence in stirred tanks: anisotropic, approximate, and applied, Can. J. Chem. Eng. 76 (1998) 563–576.
[13] V. Alopaeus, P. Moilanen, M. Laakkonen, Analysis of stirred tanks with two-zone models, AIChE J. 55 (2009) 2545–2552.
[14] G. Dompazis, V. Kanellopoulos, V. Touloupides, C. Kiparissides, Development of a multi-scale, multi-phase, multi-zone dynamic model for the prediction of

particle segregation in catalytic olefin polymerization FBRs, Chem. Eng. Sci. 63 (2007) 4735–4753.
[15] K.K. Singh, S.M. Mahajani, K.T. Shenoy, S.K. Ghosh, Population balance modeling of liquid–liquid dispersions in homogeneous continuous-flow stirred tank, Ind. Eng. Chem. Res. 48 (2009) 8121–8133.
[16] E. Vivaldo-Lima, P.E. Wood, A.E. Hamielec, A. Penlidis, Calculation of the particle size distribution in suspension polymerization using a compartment-mixing model, Can. J. Chem. Eng. 76 (1998) 495–505.
[17] V. Alopaeus, J. Koskinen, K.I. Keskinen, Simulation of the population balances for liquid–liquid systems in a nonideal stirred tank. Part 1 Description and qualitative validation of the model, Chem. Eng. Sci. 54 (1999) 5887–5899.
[18] J.C. Lasheras, C. Eastwood, C. Martinez-Bazan, J.L. Montanes, A review of statistical models for the break-up of an immiscible fluid immersed into a fully developed turbulent flow, Int. J. Multiphase Flow 28 (2002) 247–278.
[19] Y. Liao, D. Lucas, A literature review of theoretical models for drop and bubble breakup in turbulent dispersions, Chem. Eng. Sci. 64 (2009) 3389–3406.
[20] T.F. Wang, J.F. Wang, Y. Jin, A novel theoretical breakup kernel function for bubbles/droplets in a turbulent flow, Chem. Eng. Sci. 58 (2003) 4629–4637.
[21] Y. Liao, D. Lucas, A literature review on mechanisms and models for the coalescence process of fluid particles, Chem. Eng. Sci. 65 (2010) 2851–2864.
[22] C.A. Coulaloglou, L.L. Tavlarides, Description of interaction processes in agitated liquid–liquid dispersions, Chem. Eng. Sci. 32 (1977) 1289–1297.
[23] M. Martín, F.J. Montes, M.A. Galán, Theoretical modelling of the effect of surface active species on the mass transfer rates in bubble column reactors, Chem. Eng. J. 155 (2009) 272–284.
[24] P.M. Bapat, L.L. Tavlarides, G.W. Smith, Monte-Carlo simulation of mass-transfer in liquid–liquid dispersions, Chem. Eng. Sci. 38 (1983) 2003–2013.
[25] R. Andersson, B. Andersson, On the breakup of fluid particles in turbulent flows, AIChE J. 52 (2006) 2020–2030.
[26] S. Maaß, A. Gäbler, A. Zaccone, A.R. Paschedag, M. Kraume, Experimental investigations and modelling of breakage phenomena in stirred liquid/liquid systems, Chem. Eng. Res. Des. 85 (2007) 703–709.
[27] M. Wulkow, A. Gerstlauer, U. Nieken, Modeling and simulation of crystallization processes using parsival, Chem. Eng. Sci. 56 (2001) 2575–2588.
[28] J.E. Glass, Adsorption characteristics of water-soluble polymers at aqueous-organic liquid interfaces, J. Polym. Sci. Part C: Polym. Symp. 34 (1971) 141–157.
[29] M. Kraume, P. Zehner, Experience with experimental standards for measurements of various parameters in stirred tanks: a comparative test, Chem. Eng. Res. Des. 79 (2001) 811–818.
[30] S. Maaß, S. Wollny, A. Voigt, M. Kraume, Experimental comparison of measurement technique for drop size distributions in liquid/liquid dispersions, Exp. Fluids, 14 pp., in press, doi:10.1007/s00348-010-0918-9.
[31] M. Laakkonen, P. Moilanen, J. Aittamaa, Local bubble size distributions in agitated vessels, Chem. Eng. J. 106 (2005) 133–143.
[32] J. Ritter, M. Kraume, On-line measurement technique for drop size distributions in liquid/liquid systems at high dispersed phase fractions, Chem. Eng. Technol. 23 (2000) 579–582.
[33] M. Nocentini, F. Magelli, G. Pasquali, D. Fajner, A fluid-dynamic study of a gas–liquid, non-standard vessel stirred by multiple impellers, Chem. Eng. J. 37 (1988) 53–59.
[34] J. Karcz, M. Major, An effect of a baffle length on the power consumption in an agitated vessel, Chem. Eng. Process. 37 (1998) 249–256.
[35] M. Li, G. White, D. Wilkinson, K.J. Roberts, Scale up study of retreat curve impeller stirred tanks using LDA measurements and CFD simulation, Chem. Eng. J. 108 (2005) 81–90.
[36] J. Markopoulos, E. Babalona, E. Tsiliopoulou, Power consumption in agitated vessels with dual Rushton turbines: baffle length and impeller spacing effects, Chem. Eng. Technol. 27 (2004) 1212–1215.
[37] A. Gäbler, M. Wegener, A.R. Paschedag, M. Kraume, The effect of pH on experimental and simulation results of transient drop size distributions in stirred liquid–liquid dispersions, Chem. Eng. Sci. 61 (2006) 3018–3024.
[38] H. Naseef, A. Soultan, M. Stamatoudis, Effect of impeller blade height on the drop size distribution in agitated dispersions, Chem. Eng. Technol. 29 (2006) 583–587.
[39] D. Sechremeli, A. Stampouli, M. Stamatoudis, Comparison of mean drop sizes and drop size distributions in agitated liquid–liquid dispersions produced by disk and open type impellers, Chem. Eng. J. 117 (2006) 117–122.
[40] D.L. Marchisio, J.T. Pikturna, R.O. Fox, R.D. Vigil, A.A. Barresi, Quadrature method of moments for population-balance equations, AIChE J. 49 (2003) 1266–1276.